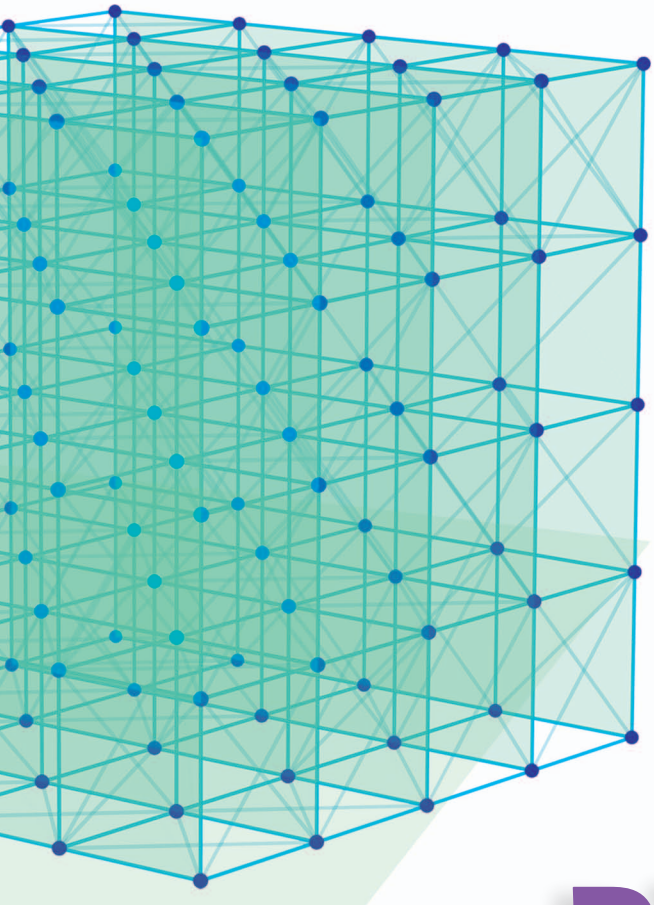

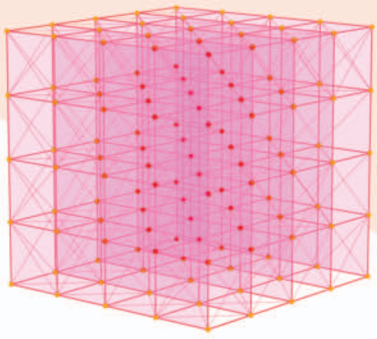

Over at least the last two decades, digital predistortion (DPD) has become the most common and widespread solution to cope with the power amplifier's (PA's) inherent linearity-versus-efficiency tradeoff. When compared with other linearization techniques, such as Cartesian feedback or feedforward, DPD has proven able to adapt to the always-growing demands of technology: wider bandwidths, stringent spectrum masks, and reconfigurability. The principles of predistortion linearization (in its analog or digital forms) are straightforward, and the linearization subsystem precedes the PA (a nonlinear function in a digital signal processor in the case of DPD or nonlinear device in the

Digital Predistorters Go Multidimensional

Pere L. Gilabert, Gabriel Montoro, David Vegas, Nieves Ruiz, and José Angel García

Pere L. Gilabert (plgilabert@tsc.upc.edu) and Gabriel Montoro (gabriel.montoro@upc.edu) are with the Department of Signal Theory and Communications, Universitat Politècnica de Catalunya, Castelldefels, Spain. David Vegas (david.vegass@unican.es), Nieves Ruiz (mariadelasnieves.ruiz@unican.es), and José Ángel García (joseangel.garcia@unican.es) are with the Department of Communications Engineering, Universidad de Cantabria, Santander, Spain.

Digital Object Identifier 10.1109/MMM.2019.2898021

Date of publication: 5 April 2019

case of analog predistortion and counteracts the nonlinear characteristic of the PA. Some excellent overviews on DPD can be found in [1]–[4]. Let us now look at the challenges that DPD linearization has faced and will continue to face in the near future with 5G new radio (5G-NR).

In mobile communications, at some point after the evolution from 2G [global system for mobile (GSM) → general packet radio service → enhanced data rates for GSM evolution (EDGE)] to 3G [wideband code division multiple access (WCDMA) → high-speed packet access (HSPA) → HSPA+] and with the advent of smartphones, mobile data consumption began its unstoppable rise. Consequently, a more efficient use of the radioelectric spectrum was required. For example, in 2G GSM-EDGE, the maximum link spectral efficiency was 1.92 b/s/Hz, but, only a few years later, 3G-HSPA achieved 4.22 b/s/Hz [5]. However, the new waveforms were optimized from the perspective of spectral efficiency, not power efficiency. New challenges arose from the power-efficiency perspective because we had to go from an efficient amplification of constant-envelope-modulation waveforms in 2G [i.e., 200-kHz bandwidth, single-carrier Gaussian minimum shift keying signals with 0 dB of peak-to-average power ratio (PAPR)] operating close to or in saturation with amplitude- and phase-modulated spread spectrum signals in 3G (i.e., a 5-MHz bandwidth WCDMA signal with 6 dB of PAPR). High-fidelity amplification of nonconstant envelope-modulated signals with high PAPR requires avoiding envelope clipping at saturation, causing operation at significant power backoff levels where PA efficiency figures are far below the maximum achievable values.

With 4G (LTE, LTE-Advanced), to satisfy the need for higher data rates and numbers of users, spectrally efficient multicarrier waveforms (i.e., 20 MHz of orthogonal frequency-division multiplexing–based signals) with high-density modulations [e.g., 64-quadrature-amplitude modulation (QAM)] were introduced. Additionally, new technologies emerged in the evolution of 4G LTE, such as carrier aggregation and multiple input/multiple output (MIMO), extending the maximum data rate up to, for example, up to 3 GB/s in LTE-advanced when considering aggregated bandwidths 100 MHz and 4 × 2 MIMO. These technologies continue to develop to massive speed and scale in 5G-NR.

In 5G-NR [6], the same network infrastructure will be able to efficiently serve different types of traffic having a very wide range of requirements, such as the huge number of users for the Internet of Things, ultralow latency and high reliability for mission-critical systems, and enhanced transmission rates for broadband mobile communications. 5G-NR is intended to provide very high data rates everywhere. To achieve this goal, bandwidths up to GHz will be allocated at millimeter-wave (mm-wave) bands, and, at sub-6 GHz, bandwidth of hundreds of MHz will be required.

Achieving these new capabilities requires coping with multiple demanding challenges that, particularly for the design of radio transceivers, are related to several factors:

1) ensuring the linearity of signals having bandwidths of several hundreds of megahertz and peak factors exceeding 10 dB to ensure high transmission rates
2) improving energy and computational efficiency, as denser deployments of base stations are expected to scale down the need for transmitted power
3) transmitting architectures with multiple antennas (massive MIMO in mm-wave bands) and multiple PAs to apply beamforming techniques that allow increasing capacity and decreasing radiated power
4) simultaneous transmission and reception (full frequency-division duplex in sub-6 GHz bands).

As mentioned, DPD can overcome, or at least mitigate, the efficiency versus linearity problem in PAs. However, the resulting power efficiency achieved with linearization techniques applied to PAs operating as controlled current sources (e.g., classes A, B, and AB) is limited. To avoid wasting excessive power resources when handling high PAPR signals, the operating conditions of a current-source-mode PA could be forced to follow its envelope, or switched-mode amplifying classes could be properly introduced. Among the set of techniques aimed at dynamic bias or load adaptation, envelope tracking (ET) [7]–[9], Doherty [10], [11], and linear amplification with nonlinear components (LINC) or outphasing PAs [12], [13] are the most widely proposed in the literature.

In addition, significant efforts have been dedicated in recent years to designing wireless communication systems capable of handling multistandard or multiband signals at the same time. The advantages of having a single PA process signals in multiple bands simultaneously are the reductions in the number of

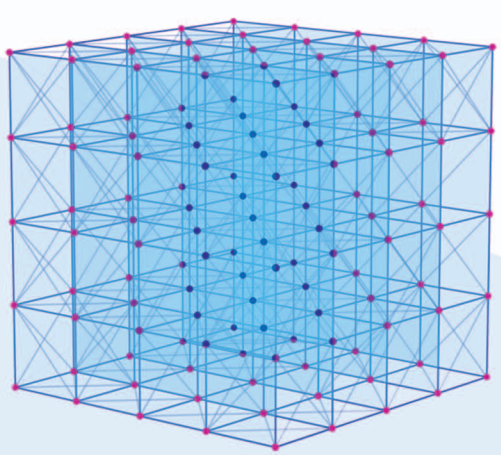

DPD can overcome, or at least mitigate, the efficiency versus linearity problem in PAs.

components and the cost of the RF subsystem [14]. For bands separated by several hundred megahertz, the implementation of a wideband DPD is not feasible, especially in real-time platforms. Fortunately, DPD systems for multiband signals can be significantly simplified, assuming that the nonlinear distortions of concern are those arising close to the band of interest and that the rest can be removed by filtering. When concurrent multiband transmissions in PAs with dynamic-load or dynamic-supply modulation are combined, the DPD needs to go multidimensional. That is, multiple input/single output (MISO) DPD behavioral models are necessary to compensate for all of the unwanted distortion effects that appear at the PA output.

Similarly, in multiantenna systems where each transmit path has its own PA and antenna element, bulky components, such as isolators (placed between the PA and the antenna), are removed to avoid increasing the system complexity and cost. As a consequence, these integrated, multiantenna transmitters typically suffer from nonlinear distortion because of mixing of the antenna crosstalk and mismatch with the PA output, in addition to the nonlinear distortion caused by the PAs [15]. This is another example in which DPD needs to go multidimensional to compensate for the multiple sources of unwanted distortion effects.

Figure 1 shows a conceptual map or compact overview of the previously mentioned applications where multidimensional DPD is used and identifies some references, research groups, and companies that have published on these topics. This article focuses on the multidimensional DPD required to compensate for concurrent multiband transmission when using dynamic-load or dynamic-supply-modulated PAs. ET and outphasing PAs are unlikely to be deployed for ultrawideband applications in 5G mm-wave bands because of the bandwidth and power/cost budget limitations of these high-efficiency amplification architectures, which require DPD linearization. However, in 5G sub-6-GHz macro base stations, if envelope bandwidth or

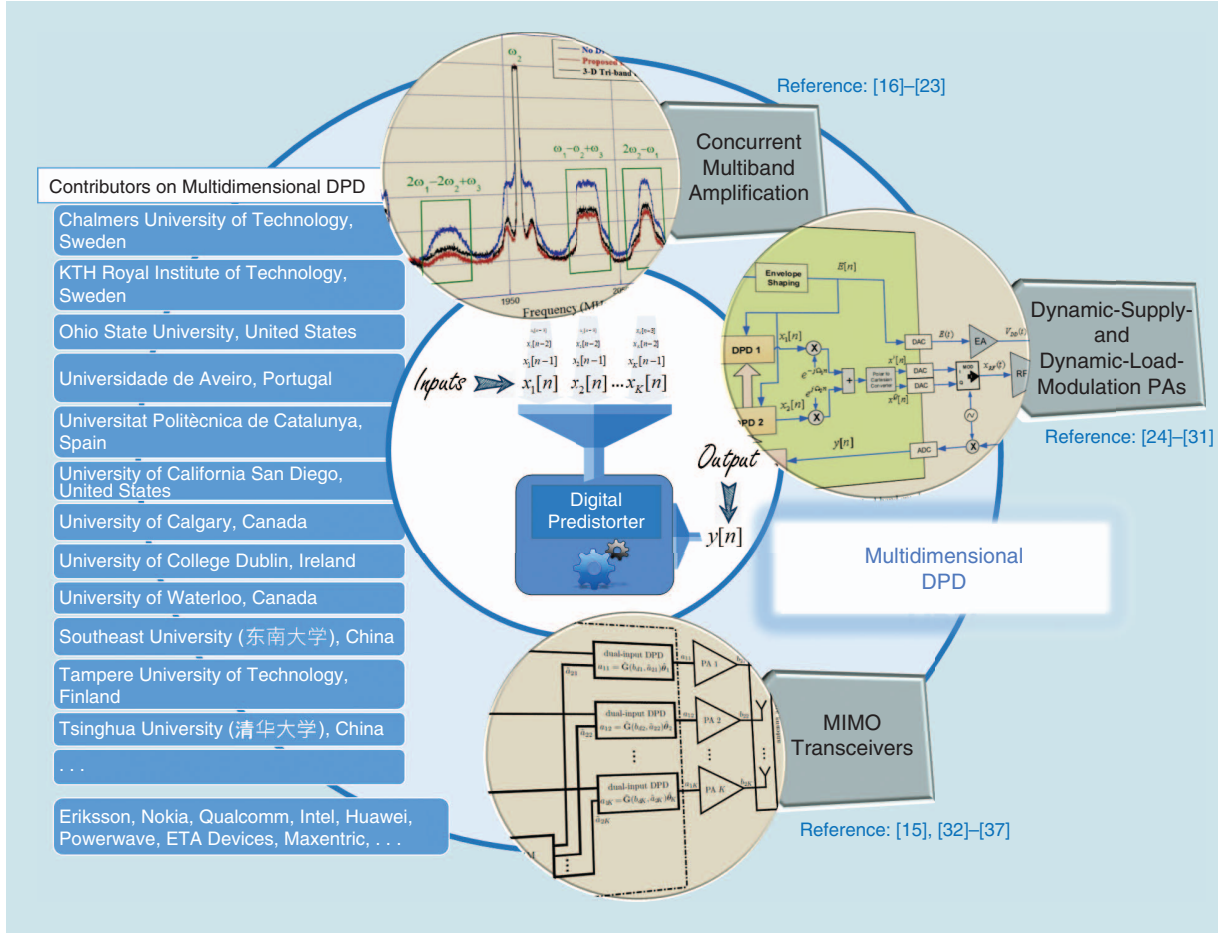

Figure 1. *The applications for multidimensional DPD models (MISO DPD) [15], [17], [26].*

slew-rate reduction techniques [25] properly combined with dimensionality reduction techniques [30] are considered to meet the low complexity requirements of the DPD implementation, the use of dynamic-supply- (e.g., ET or class-G PAs) or dynamic-load-modulation techniques (e.g., outphasing or load-modulated-balanced PAs) can still be seen as interesting solutions for high-efficiency amplification.

DPD for PAs With Dynamic-Supply or Dynamic-Load Modulation in Concurrent Multiband Transmissions

Dynamic-Supply Versus Dynamic-Load Modulation

In ET PAs, the supply voltage of the RF PA is adjusted according to the envelope of the RF carrier. Thanks to the dynamic supply, the RF PA (linear current-source mode, Doherty, or even LINC PAs) can be forced to operate close to saturation, which increases the power efficiency at power backoff. Several strategies can be designed (through the so-called shaping function) to shape the supply voltage signal to achieve better linearity and efficiency or to meet the slew-rate and bandwidth restrictions of the drain modulator [7]–[9].

In outphasing PAs [12], [13], the idea introduced by H. Chireix was to use phase control of two constituent branch PAs operated in saturation by enabling constant-output envelope signals that were summed at the output of the system to allow AM. The concept was later reintroduced by D.C. Cox, who generalized the linear amplification with nonlinear components (i.e., LINC) approach. The main difference is that, although the Chireix combiner is nonisolating (and, therefore, the output signal from each PA changes the load impedance seen by the other), providing good efficiency but not-so-good linearity, the LINC combiner isolates the two PA outputs (allowing them to see a fixed load at all times), which favors having good combining linearity but leads to high dissipation at high outphasing angles.

In ET PAs, the supply voltage of the RF PA is adjusted according to the envelope of the RF carrier.

If the PAs are assumed to operate as ideal voltage sources, with their outputs connected to a floating load R (usually provided by a balun), as the relative phase between the two sources is varied between 180° and 0°, the effective loading on both PAs is varied between $R/2$ and infinity. The output power from each branch PA is decreased, thereby reducing the dissipated power losses [12]. This is the principle of the concept of active-load modulation proposed by Chireix, who also added two fixed compensating reactances to provide some control over the efficiency-versus-output power profile.

The concepts of dynamic-supply and active-load modulation can be appreciated based on Figure 2, which shows the gain and efficiency evolution versus the output power for different supply voltages [Figure 2(a)] and different outphasing angles [Figure 2(b)] when characterizing one single or two reactively combined continuous class-J mode gallium nitride (GaN) high-electron mobility transistor PAs, respectively [38]. For ET, the Nujira company (acquired by Qualcomm) introduced the concept of isogain shaping [39], whereby the instantaneous supply voltage is designed to achieve a particular constant

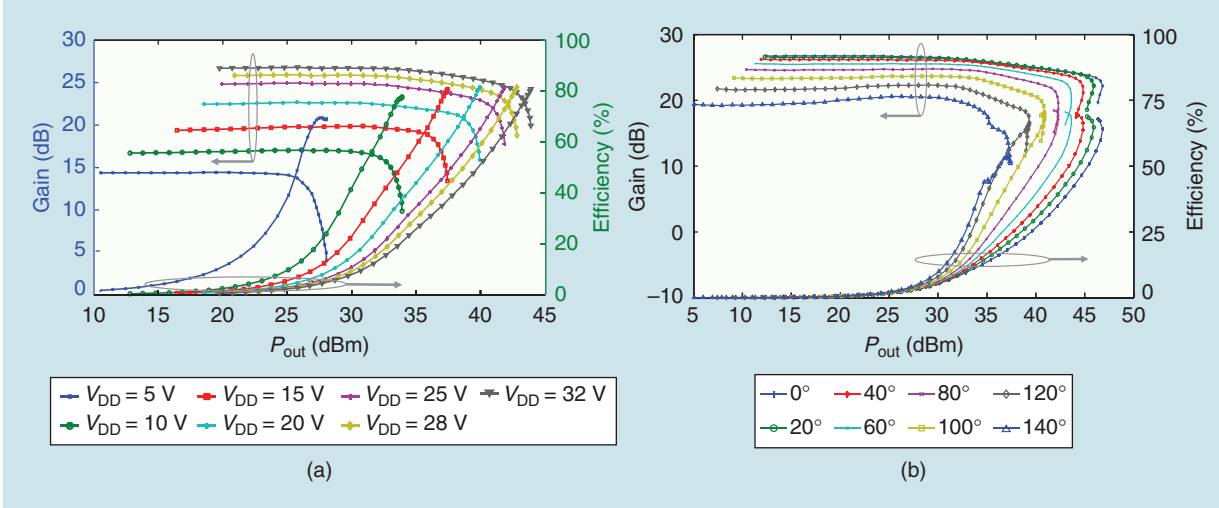

Figure 2. *The gain and efficiency evolution versus output power: (a) at $V_{GS} = -2.3$ V and $R_L = 50\ \Omega$ for different V_{DD} values and (b) for different outphasing angles.*

The isogain trajectory provides constant gain at the price of losing certain efficiency versus the optimum efficiency trajectory.

PA gain. In this case, the ET PA system achieves low AM/AM distortion at the price of lower efficiency than when optimized. In a similar fashion, the isogain approach can be applied in outphasing systems [38] or alternative dynamic-load-modulation techniques, as shown in Figure 3, where the gain [Figure 3(a)] and efficiency [Figure 3(b)] evolution versus output power with a single PA is shown for different resistive loading values. The isogain trajectory provides constant gain at the price of losing certain efficiency versus the optimum efficiency trajectory. In the following section, we particularize the shaping of the supply voltage in ET PAs and the outphasing angle in outphasing PAs when considering concurrent multiband transmissions.

Slow-Envelope Generation in Multiband Transmission

The amplification of concurrent multiband or even carrier-aggregated transmissions with high-efficiency topologies based on dynamic-supply modulation (e.g., ET) or dynamic-load modulation (e.g., outphasing) faces several challenges. On the one hand, to guarantee the desired linearity levels, the DPD must be designed to account for the difficulty of running the DPD at approximately five times the signal instantaneous bandwidth (due to bandwidth expansion occurring during the DPD process). For bands separated by several hundreds of megahertz, the implementation of a wideband DPD is not feasible, especially in real-time platforms. Fortunately, DPD systems for multiband signals can be significantly simplified, assuming that the nonlinear distortions of concern are those that arise close to the band of interest and that the rest can be removed by filtering.

On the other hand, both dynamic-supply- and dynamic-load-modulation techniques are capable of achieving high power-efficiency figures even when operated with amplitude- and phase-modulated signals presenting significant PAPR (i.e., good efficiency profiles with backoff operation). However, the efficiency decays with the signal's bandwidth. Both dynamic techniques show a tradeoff between the mean power efficiency that can be achieved and the instantaneous signal bandwidth handled by the PA.

A Chireix outphasing PA is intrinsically narrowband. The frequency-dependent characteristic of the nonisolating combiner, including the compensating reactances, and the reactive elements in the device model usually impose strong limitations on its bandwidth. For example, if designed with class-E switched-mode PAs (a highly attractive operating class in terms of efficiency performance), the efficiency contours rotate counterclockwise with increasing frequency, whereas the mutual-load-modulation trajectories offered by a passive (Foster) combiner rotate in the expected clockwise sense [40]. In a pure outphasing operation, the constant-envelope phase-modulated signals to be handled by the constitutive branches may have a bandwidth several times wider than the original signal to be reproduced. For wideband or multiband signals, a broadband input matching network would also be required to avoid undesired phase-modulation-to-AM conversion. In ET PAs, one of the main challenges involves the design of efficient envelope modulators capable of supplying the power required by

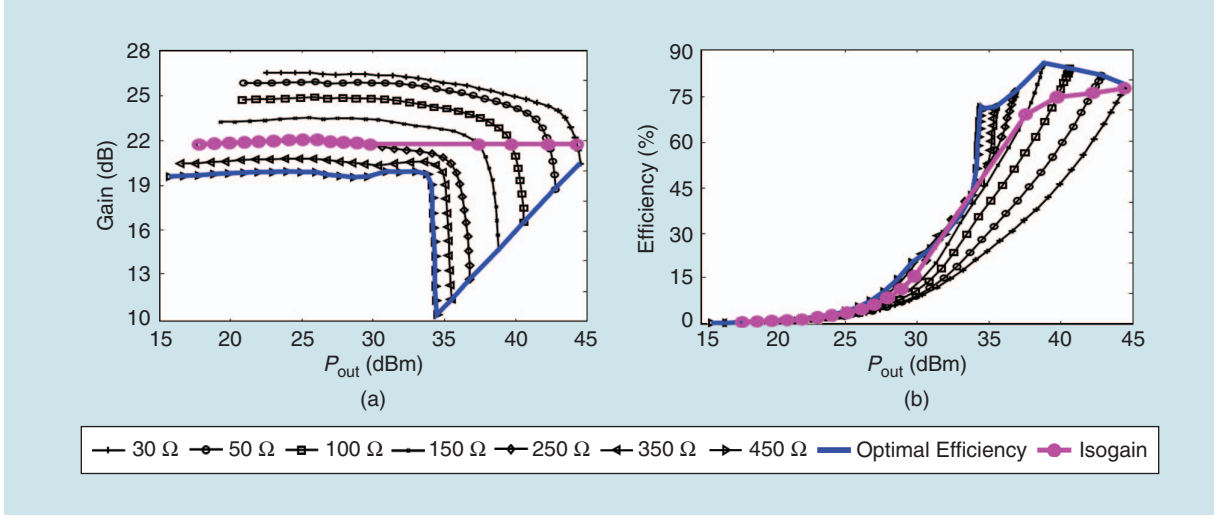

Figure 3. *The (a) gain and (b) efficiency evolution versus output power at $V_{GS} = -2.3$ V and $V_{DD} = 28$ V for different R_L values.*

the transistor at the same speed as the signal's envelope. In concurrent multiband transmission, the envelope of the resulting RF signal can present bandwidths that are several times (according to the rule of thumb, approximately three times) the instantaneous bandwidth. For example, with carriers separated by hundreds of megahertz, the envelope modulator should present a slew rate capable of efficiently amplifying the supply signals of gigahertz of bandwidth. Currently, commercial envelope drivers for base stations can efficiently handle signal bandwidths up to 40 MHz with power efficiencies greater than 70% [41].

Because the efficiency of the envelope modulator drops at high frequencies, to avoid dealing with high-speed envelope variations in multiband signals, methods to reduce the bandwidth [24] or slew rate [25] of the signal's envelope have been proposed. In addition, in the particular case of dual-band signals, two main

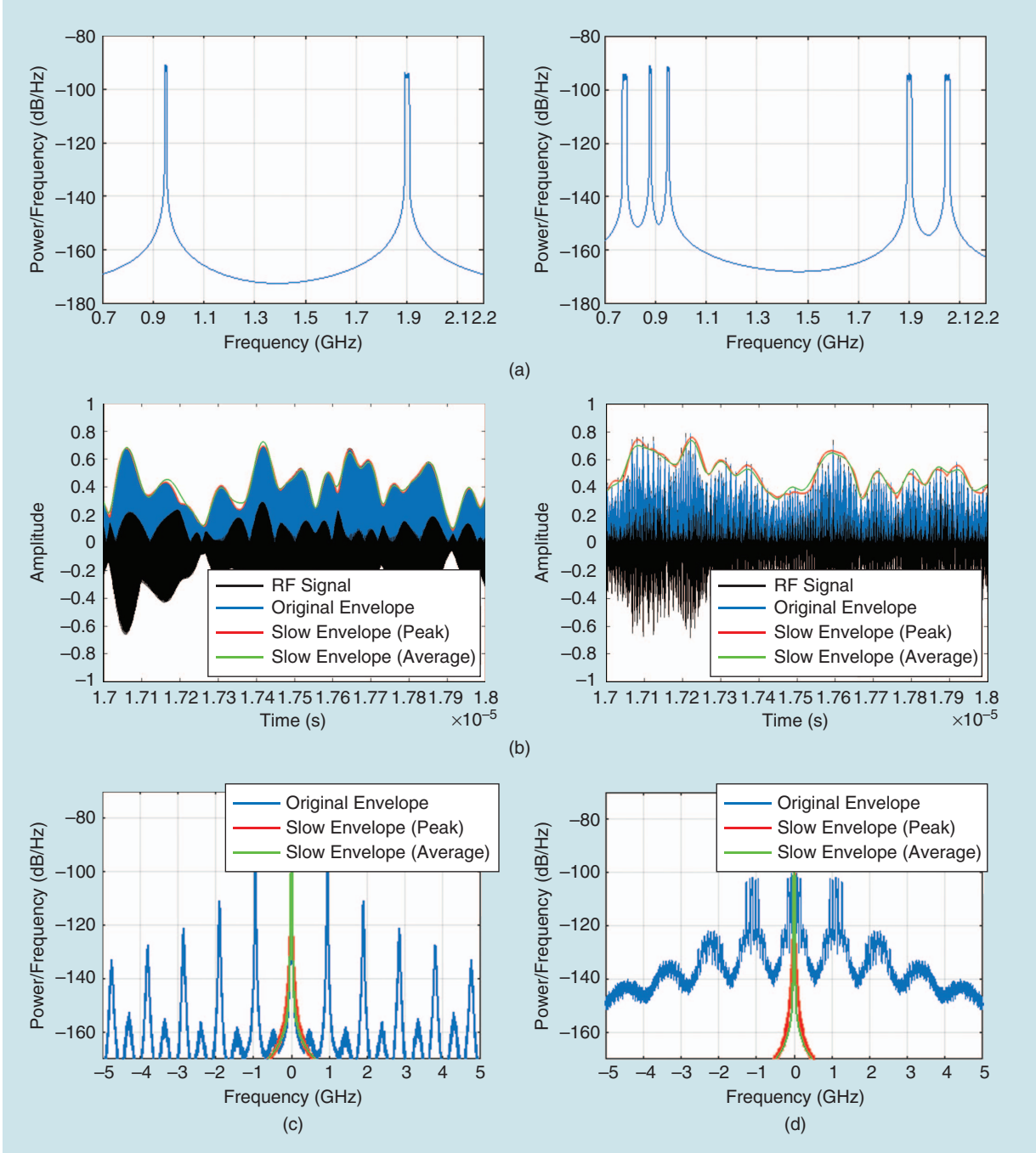

Figure 4. *The (a) spectra of the RF signal, (b) slow-envelope waveforms (peak [p = 1] and average [p = 2] approaches), and slow-envelope spectra of both the (c) dual-band (m = 2) and (d) multiband transmissions (m = 5).*

At deep power backoff, there may be no benefit in terms of power-added efficiency when operating in a pure outphasing mode.

approaches to deal with the instantaneous dual-band envelope of the transmitted signal have been described: 1) perform the sum of the modulus of the baseband signals [i.e., the peak of the instantaneous dual-band envelope, $p=1$ in (1)], as proposed in [26]; or 2) perform the square root of the sum of the squared modulus of the baseband signals [i.e., the average amplitude of the instantaneous dual-band envelope, $p=2$ in (1)], as proposed in [28]. These two approaches are particular solutions of the following method that can be generalized for multiband transmissions. Therefore, to generate a slower envelope version $E_S[n]$ of the original instantaneous envelope $|u[n]|$, the generalized mean or power mean with exponent p can be extended for m bands,

$$E_S[n]=\left(\frac{1}{m}\sum_{i=1}^{m}|u_i[n]|^p\right)^{\frac{1}{p}}, \tag{1}$$

where the multiband complex baseband signal is defined as

$$u[n]=\sum_{i=1}^{m}u_i[n]e^{j\Omega_i n}, \tag{2}$$

where $\Omega_i=2\pi f_i/f_s$ and f_i and f_s are the center frequency and the sampling frequency, respectively.

Figure 4 shows the time-domain waveforms and spectra of the original RF signal's envelope and two examples of slow-envelope generation (peak, $p=1$, and average, $p=2$, approaches) when considering a dual-band ($m=2$) and a multiband transmission ($m=5$). The generated slow envelope then goes through a shaping function (a comparison of different shaping functions can be found in [7]), which, in the case of multiband transmissions, consists of a detroughing function. Detroughing prevents the supply signal $V_{DD}(t)$ from dropping to zero volts, thus avoiding sharp amplitude nulls in the time domain that may increase the bandwidth requirements. Moreover, a supply is typically more efficient at higher voltage levels and with a limited voltage swing, whereas at low power levels the efficiency is not as important. Figure 5 depicts two different shaping functions: hard and soft detroughing. Soft detroughing can be defined with a function as described in [42],

$$E[n]=\left((E_{S\_TH})^6+(E_S[n])^6\right)^{\frac{1}{6}}, \tag{3}$$

where E_{S_TH} determines the shaping curve and the minimum clipping level.

Multidimensional DPD

Dealing with signals presenting instantaneous bandwidths of several hundreds of megahertz is a challenge. This is true not only for analog-to-digital converters (ADCs) and digital-to-analog converters (DACs) that need to operate with sampling rates at least five times the signal's instantaneous bandwidth (note that, despite using undersampling techniques for the ADC [1], the DAC at least has to operate at full rate). It is also true because the field-programmable gate array (FPGA) must operate at clock rates that, being optimistic, may be at the limit of current technology (e.g., current commercially available intellectual property for DPD are limited to signal bandwidths up to 200 MHz). In multiband signals, we can relax the clock rate constraints, assuming that the nonlinear distortions of concern are

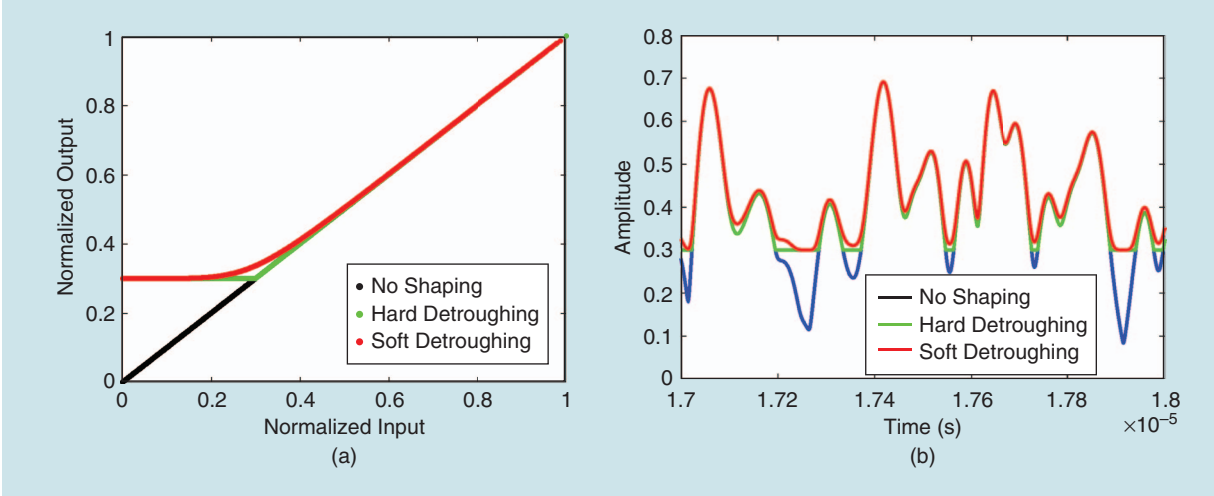

Figure 5. *The (a) detroughing shaping functions and (b) waveforms before and after detroughing.*

those that arise close to the band of interest and, thus, that individual DPDs will take care of each multiband transmission.

As explained, several MISO DPD models have been published that compensate not only for the intraband intermodulation distortion (both in-band and out-of-band distortion) but also for the crossband-intermodulation distortion (Figure 1). In addition, using a significantly slower envelope than the original instantaneous multiband envelope to dynamically supply or dynamically load-modulate the PA will introduce additional nonlinear distortion. Consequently, to compensate for the slow-envelope-dependent distortion effects, we need a concurrent multiband DPD model that includes the information of the slow envelope,

$$x_i[n] = f_{\mathrm{DPD},i}(u_1[n], u_2[n], \ldots, u_K[n], E[n], n), \quad (4)$$

where $x_i[n]$ with $i = 1, 2, \ldots, K$ is the ith output of the MISO DPD; $u_1[n], u_2[n], \ldots, u_K[n]$ are multiple inputs corresponding to each of the concurrent bands; and $E[n]$ is the generated slow envelope. Thus, the baseband signal processing for generating the predistorted in-phase/quadrature (I/Q) signals is the same for both ET and outphasing PAs (which are considered black-box systems) and consists of the MISO system described in (4), with as many input signals as concurrent bands and the slow-envelope signal used to dynamically supply the PA or code the outphasing angle.

Figure 6 shows a block diagram of a multidimensional DPD to compensate for the intraband, crossband, and slow-envelope-dependent distortion effects in a concurrent multiband system when considering either dynamic-load modulation (i.e., outphasing PA) or dynamic-supply modulation (i.e., ET PA). In the case

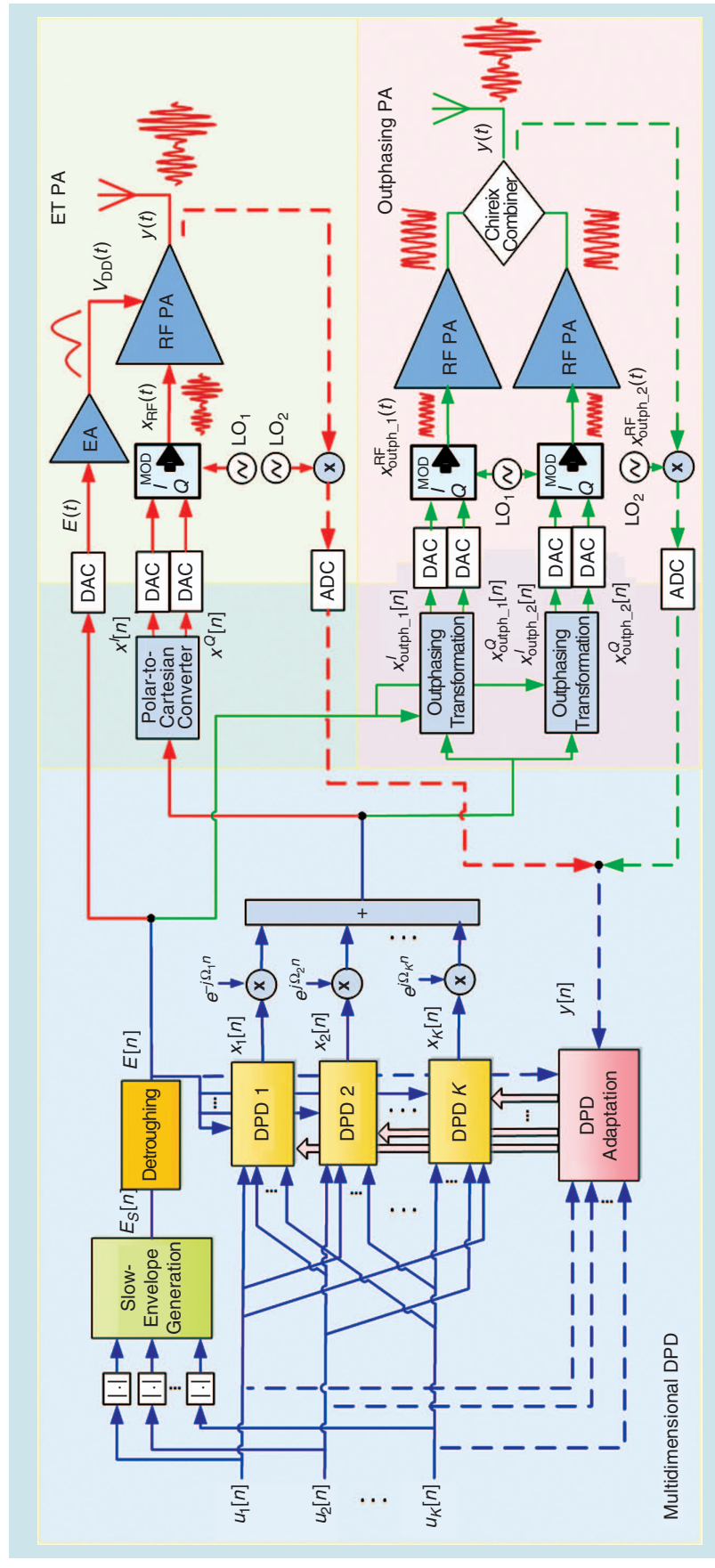

Figure 6. *A block diagram of a multidimensional DPD for both ET and outphasing PAs. MOD: modulator; EA: envelope amplifier.*

of the outphasing PA, the outphasing angle coding and the calibration of the gain and phase mismatch of the two signal paths are carried out in the outphasing transformation block. Additionally, the time alignment between the RF signal and the supply-modulated signal is carried out in the slow-envelope generation block. Finally, the time-alignment and amplitude normalization between the input/output I/Q signals is done in the DPD adaptation block.

Experimental Results: ET and Outphasing PAs in a Concurrent Dual-Band Transmission

Let us now investigate an example of the general block diagram in Figure 6 for the specific case of a concurrent dual-band transmission. Figure 7 shows the structure of the proposed 3D distributed memory polynomial (DMP) model presented in [26], which includes three branches to compensate for in-band, out-of-band, and crossband-intermodulation distortion and slow-envelope distortion, respectively.

This particular 3D DPD model was used in a concurrent dual-band transmission in [26] and [30] to compensate for the unwanted nonlinear distortion of an ET PA. For example, Figure 8(a) shows the output spectra of an ET PA used in [30] before and after 3D DPD. Using the slow envelope to dynamically supply the PA is a suboptimal solution from the power-efficiency point of view when compared with using the original RF signal's envelope. However, it is the only feasible solution, considering the drain modulator's bandwidth limitations. Moreover, this approach is always more efficient than considering a fixed supply. Figure 9 (top) summarizes the results presented in [26] for a concurrent, dual-band ET PA where, even using the slow envelope (with both peak and average approaches) to dynamically supply the PA, we can double the drain efficiency compared with the fixed supply. In addition, the adjacent channel leakage ratio threshold of –45 dB relative to carrier is guaranteed by applying 3D DPD linearization with fewer than 100 coefficients [26].

Let us go back to the general block diagram in Figure 6 to consider concurrent dual-band outphasing amplification. In particular, we look at mixed- or hybrid-mode outphasing

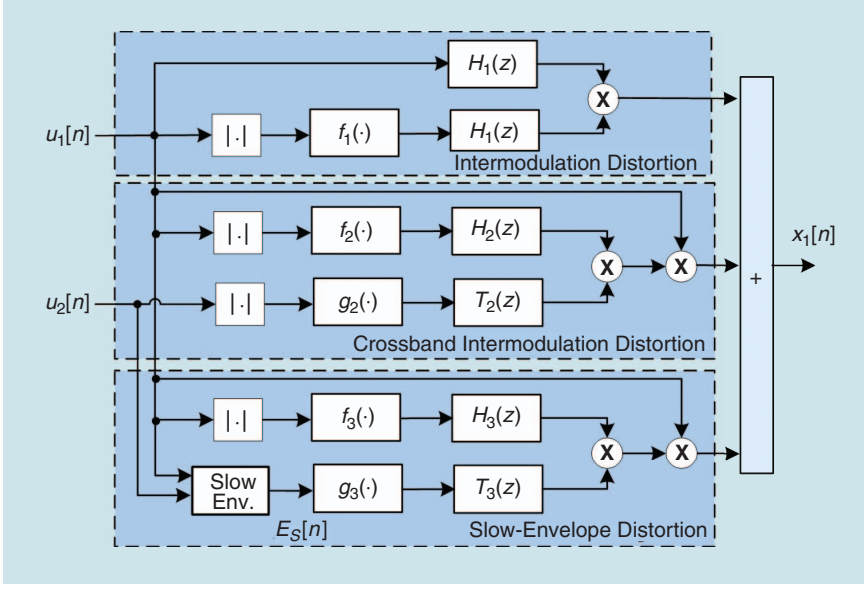

Figure 7. *The structure of the proposed 3D DMP DPD for band 1.*

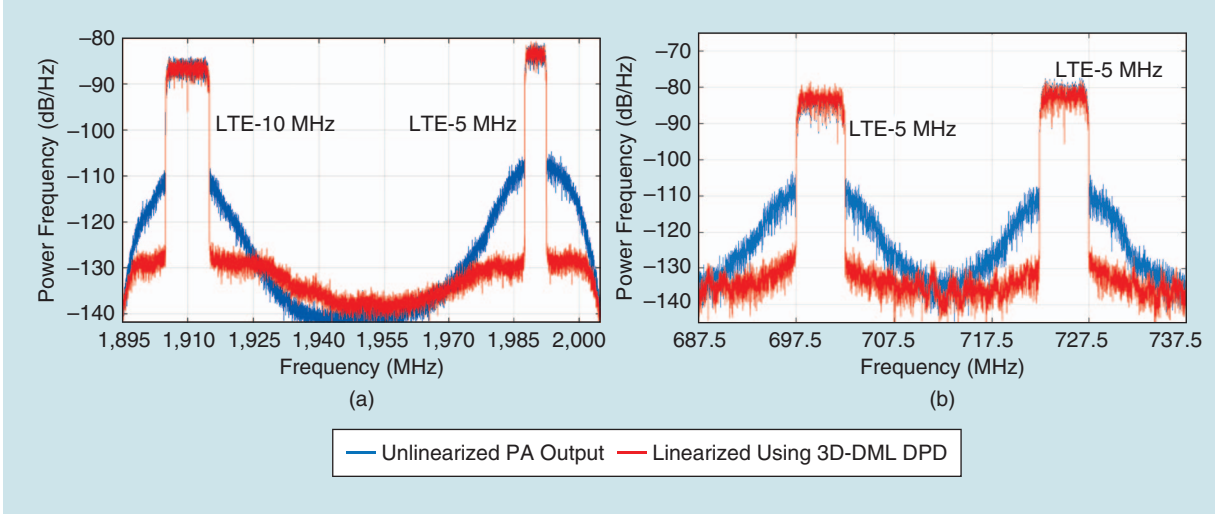

Figure 8. *The unlinearized and 3D DPD linearized output spectra of (a) an ET PA [26] and (b) a hybrid outphasing PA.*

amplification [43] because we allow some amplitude variation in the phase-modulated outphasing components. This hybrid approach helps mitigate the bandwidth expansion that occurs when amplifying pure constant-amplitude phase-modulated components. In this way, the hybrid-outphasing PA becomes more linearizable, even if at the price of slightly degrading power efficiency. In fact, at deep power backoff, there may be no benefit in terms of power-added efficiency when operating in a pure outphasing mode. Therefore, both hybrid outphasing signal components can be defined at baseband as

$$x_{\text{outph\_1}}[n] = A[n]e^{j(\varphi_x[n]+\alpha[n])} = x^I_{\text{outph\_1}}[n] + jx^Q_{\text{outph\_1}}[n] \quad (5)$$

and

$$x_{\text{outph\_2}}[n] = A[n]e^{j(\varphi_x[n]-\alpha[n])} = x^I_{\text{outph\_2}}[n] + jx^Q_{\text{outph\_2}}[n], \quad (6)$$

where half of the outphasing angle, $\alpha[n]$, is defined as a function of the slow envelope $\alpha[n] = f(E[n])$, $\varphi_x[n]$ is the original instantaneous phase of the dual-band signal, and $A[n]$ is the amplitude of the hybrid or mixed-mode outphasing components and, unlike the pure outphasing components, some amplitude variation is allowed: $A[n] = (x[n]/E[n]) \cdot \beta$, with $0 < \beta < 1$.

Figure 8(a) shows the dual-band output spectra of a hybrid outphasing PA before and after 3D DPD linearization where, again, dimensionality reduction

DPD is a linearization technique par excellence that deals with the inherent PA linearity-versus-power efficiency tradeoff.

techniques are applied to keep the number of coefficients below 100. On the one hand, to select the most relevant basis of the DPD function in the forward path, a greedy algorithm, such as, the orthogonal matching pursuit [30], [44], can be used. On the other hand, feature-extraction techniques, such as principal component analysis [45] or the partial least squares [30], can be used to reduce the number of bases in the adaptation subsystem. Figure 9 (bottom) shows that, even with the slow envelope, the efficiency doubles compared with not applying any kind of dynamic-load modulation. By coding the slow envelope into the outphasing angle, an efficient, concurrent dual-band transmission could be feasible using a dual-band Chireix topology [46], [47], with a much less demanding implementation than the wideband counterpart, which would be required if coding the original envelope.

To validate the closed-loop DPD algorithms, a common solution as a step to a future real-time implementation is the use of a hardware-in-the-loop architecture, such as the ones shown in Figure 10. In a PC-controlled

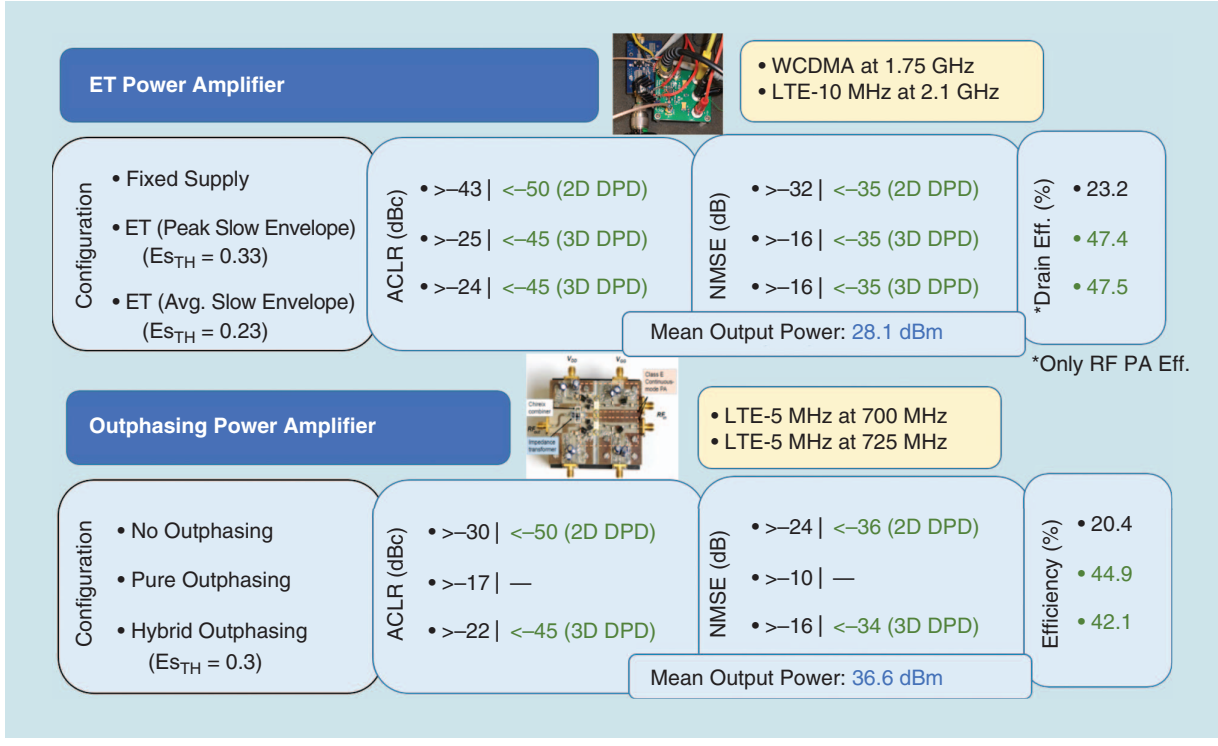

Figure 9. *The 3D DPD linearization of concurrent dual-band transmission for both ET [26] and outphasing PAs. dBc: decibels relative to the carrier; dBm: dB-mW; NMSE: normalized mean square error; ACLR: adjacent channel leakage ratio.*

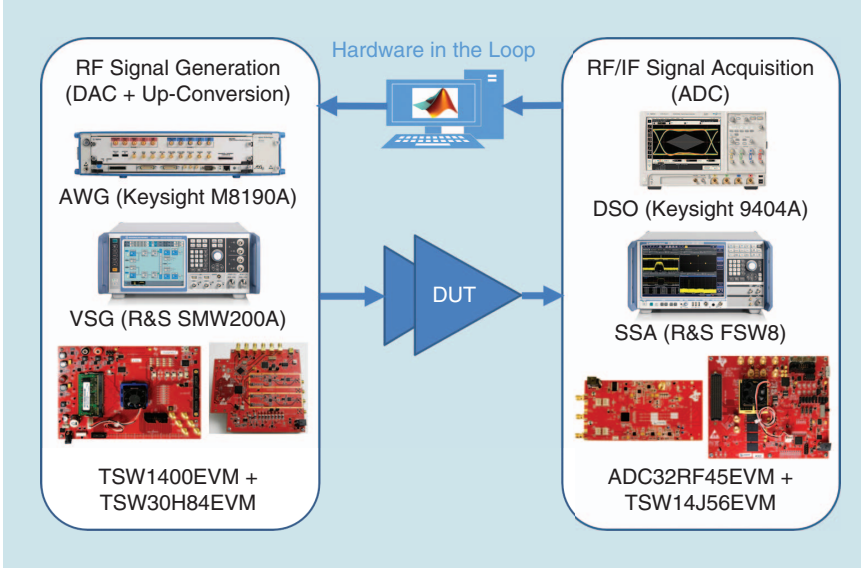

Figure 10. *The hardware-in-the-loop general architecture. DSO: digital storage oscilloscope; DUT: device under test; IF: intermediate frequency; VSG: vector signal generator; SSA: signal and spectrum analyzer; DSO: digital storage oscilloscope.*

system, the digital signal processing is carried out in MATLAB. Then, instrumentation or commercial off-the-shelf boards are used to both generate (DAC) and up-convert the RF signal to be amplified and, after going through the PA, down-convert and/or digitize (ADC) the feedback signal.

Conclusions

DPD is a linearization technique par excellence that deals with the inherent PA linearity-versus-power efficiency tradeoff. In the last decade, DPD has gone multidimensional to address new linearity challenges that have arisen due to the inclusion of techniques oriented toward maximizing spectral efficiency, such as concurrent multiband or carrier-aggregated transmissions and MIMO and the adoption of high-power-efficient architectures based on dynamic-supply or dynamic-load modulation of the PA. For multiband transmission in ET or outphasing PAs, we have shown that one strategy to cope with the bandwidth limitations of both amplification architectures uses a slower version of the original RF signal's envelope to both dynamically supply and load-modulate the PA. Finally, results considering a concurrent dual-band transmission have shown that power efficiency values can be significantly enhanced in ET and outphasing PAs by using slow envelopes and 3D DPD to compensate for the unwanted PA linear and nonlinear effects.

Acknowledgments

This work was supported in part by the Spanish Government and the Fonds Européen de Développement Économique et Régional (European Fund for Economic and Regional Development) under the Ministerio de Ciencia, Innovación y Universidades projects TEC2017-83343-C4-1-R and TEC2017-83343-C4-2-R and by the Generalitat de Catalunya under grant 2017 SGR 813.

References

[1] R. N. Braithwaite, "General principles and design overview of digital pre-distortion," in *Digital Front-End in Wireless Communications and Broadcasting*, F.-L. Luo, Ed. Cambridge, U.K.: Cambridge Univ. Press, 2011.

[2] J. Wood, "System-level design considerations for digital pre-distortion of wireless base station transmitters," *IEEE Trans. Microw. Theory Techn.*, vol. 65, no. 5, pp. 1880–1890, May 2017. doi: 10.1109/TMTT.2017.2659738.

[3] A. Katz, J. Wood, and D. Chokola, "The evolution of PA linearization: From classic feedforward and feedback through analog and digital predistortion," *IEEE Microw. Mag.*, vol. 17, no. 2, pp. 32–40, Feb. 2016. doi: 10.1109/MMM.2015.2498079.

[4] L. Guan and A. Zhu, "Green communications: Digital predistortion for wideband RF power amplifiers," *IEEE Microw. Mag.*, vol. 15, no. 7, pp. 84–99, Nov.-Dec. 2014. doi: 10.1109/MMM.2014.2356037.

[5] P. Rysavy, "Challenges and considerations in defining spectrum efficiency," in *Proc. IEEE*, vol. 102, no. 3, pp. 386–392, Mar. 2014. doi: 10.1109/JPROC.2014.2301637.

[6] K. Sundhar and L. C. Miller, *5G for Dummies*, Hoboken, NJ: Wiley, 2017.

[7] Z. Wang, "Demystifying envelope tracking: Use for high-efficiency power amplifiers for 4G and beyond," *IEEE Microw. Mag.*, vol. 16, no. 3, pp. 106–129, Apr. 2015. doi: 10.1109/MMM.2014.2385351.

[8] Z. Popovic, "Amping up the PA for 5G: Efficient GaN power amplifiers with dynamic supplies," *IEEE Microw. Mag.*, vol. 18, no. 3, pp. 137–149, May 2017. doi: 10.1109/MMM.2017.2664018.

[9] G. T. Watkins and K. Mimis, "How not to rely on Moore's law alone: Low-complexity envelope-tracking amplifiers," *IEEE Microw. Mag.*, vol. 19, no. 4, pp. 84–94, June 2018. doi: 10.1109/MMM.2018.2813840.

[10] R. Pengelly, C. Fager, and M. Ozen, "Doherty's legacy: A history of the Doherty power amplifier from 1936 to the present day," *IEEE Microw. Mag.*, vol. 17, no. 2, pp. 41–58, Feb. 2016. doi: 10.1109/MMM.2015.2498081.

[11] R. Darraji, P. Mousavi, and F. M. Ghannouchi, "Doherty goes digital: Digitally enhanced Doherty power amplifiers," *IEEE Microw. Mag.*, vol. 17, no. 8, pp. 41–51, Aug. 2016. doi: 10.1109/MMM.2016.2561478.

[12] T. Barton, "Not just a phase: Outphasing power amplifiers," *IEEE Microw. Mag.*, vol. 17, no. 2, pp. 18–31, Feb. 2016. doi: 10.1109/MMM.2015.2498078.

[13] Z. Popovic and J. A. Garcia, "Microwave class-E power amplifiers: A brief review of essential concepts in high-frequency class-E PAs and related circuits," *IEEE Microw. Mag.*, vol. 19, no. 5, pp. 54–66, July-Aug. 2018. doi: 10.1109/MMM.2018.2822202.

[14] P. Roblin, C. Quindroit, N. Naraharisetti, S. Gheitanchi, and M. Fitton, "Concurrent linearization: The state of the art for modeling and linearization of multiband power amplifiers," *IEEE Microw. Mag.*, vol. 14, no. 7, pp. 75–91, Nov. 2013. doi: 10.1109/MMM.2013.2281297.

[15] K. Hausmair, P. N. Landin, U. Gustavsson, C. Fager, and T. Eriksson, "Digital predistortion for multi-antenna transmitters affected

by antenna crosstalk," *IEEE Trans. Microw. Theory Techn.*, vol. 66, no. 3, pp. 1524–1535, Mar. 2018. doi: 10.1109/TMTT.2017.2748948.

[16] C. Yu, W. Cao, Y. Guo, and A. Zhu, "Digital compensation for transmitter leakage in non-contiguous carrier aggregation applications with FPGA implementation," *IEEE Trans. Microw. Theory Techn.*, vol. 63, no. 12, pp. 4306–4318, Dec. 2015. doi: 10.1109/TMTT.2015.2495144.

[17] M. Younes, A. Kwan, M. Rawat, and F. M. Ghannouchi, "Linearization of concurrent tri-band transmitters using 3-D phase-aligned pruned Volterra model," *IEEE Trans. Microw. Theory Techn.*, vol. 61, no. 12, pp. 4569–4578, Dec. 2013. doi: 10.1109/TMTT.2013.2287176.

[18] S. Amin, P. Händel, and D. Rönnow, "Digital predistortion of single and concurrent dual-band radio frequency GaN amplifiers with strong nonlinear memory effects," *IEEE Trans. Microw. Theory Techn.*, vol. 65, no. 7, pp. 2453–2464, July 2017. doi: 10.1109/TMTT.2016.2642948.

[19] A. Molina, K. Rajamani, and K. Azadet, "Concurrent dual-band digital predistortion using 2-D lookup tables with bilinear interpolation and extrapolation: Direct least squares coefficient adaptation," *IEEE Trans. Microw. Theory Techn.*, vol. 65, no. 4, pp. 1381–1393, Apr. 2017. doi: 10.1109/TMTT.2016.2634001.

[20] S. A. Bassam, M. Helaoui, and F. M. Ghannouchi, "2-D digital predistortion (2-D-DPD) architecture for concurrent dual-band transmitters," *IEEE Trans. Microw. Theory Techn.*, vol. 59, pp. 2547–2553, Oct. 2011. doi: 10.1109/TMTT.2011.2163802.

[21] F. Mkadem, A. Islam, and S. Boumaiza, "Multi-band complexity-reduced generalized-memory-polynomial power-amplifier digital predistortion," *IEEE Trans. Microw. Theory Techn.*, vol. 64, no. 6, pp. 1763–1774, June 2016. doi: 10.1109/TMTT.2016.2561279.

[22] W. Chen et al., "Design and linearization of concurrent dual-band Doherty power amplifier with frequency-dependent power ranges," *IEEE Trans. Microw. Theory Tech*, vol. 59, no. 10, pp. 2537–2546, 2011. doi: 10.1109/TMTT.2011.2164089.

[23] R. N. Braithwaite, "Digital predistortion of a power amplifier for signals comprising widely spaced carriers," in *Proc. 78th Microwave Measurement Symp. (ARFTG)*, 2011, pp. 1–4.

[24] J. Jeong, D. Kimball, M. Kwak, C. Hsia, P. Draxler, and P. Asbeck, "Wideband envelope tracking power amplifiers with reduced bandwidth power supply waveforms and adaptive digital predistortion techniques," *IEEE Trans. Microw. Theory Techn.*, vol. 57, no. 12, pp. 3307–3314, Dec. 2009.

[25] G. Montoro, P. L. Gilabert, J. Berenguer, and E. Bertran, "Digital predistortion of envelope tracking amplifiers driven by slew-rate limited envelopes," in *2011 IEEE MTT-S Int. Microwave Symp. Dig. (IMS)*, June 2011, pp. 1–3. doi: 10.1109/MWSYM.2011.5972693.

[26] P. L. Gilabert and G. Montoro, "3-D distributed memory polynomial behavioral model for concurrent dual-band envelope tracking power amplifier linearization," *IEEE Trans. Microw. Theory Techn.*, vol. 63, no. 2, pp. 638–648, Feb. 2015. doi: 10.1109/TMTT.2014.2387825.

[27] H. Sarbishaei, Y Hu, B. Fehri, and S. Boumaiza, "Concurrent dual-band envelope tracking power amplifier for carrier aggregated systems," in *2014 IEEE MTT-S Int. Microwave Symp. (IMS2014)*, Tampa, FL, 2014, pp. 1–4.

[28] Y. Lin, C. Quindroit, H. Jang, and P. Roblin, "3-D Fourier series based digital predistortion technique for concurrent dual-band envelope tracking with reduced envelope bandwidth," *IEEE Trans. Microw. Theory Techn.*, vol. 63, no. 9, pp. 2764–2775, Sept. 2015. doi: 10.1109/TMTT.2015.2452271.

[29] A. K. Kwan, M. Younes, R. Darraji, and F. M. Ghannouchi, "On track for efficiency: Concurrent multiband envelope-tracking power amplifiers," *IEEE Microw. Mag.*, vol. 17, no. 5, pp. 46–59, May 2016. doi: 10.1109/MMM.2016.2525118.

[30] Q. A. Pham, D. López-Bueno, T. Wang, G. Montoro, and P. L. Gilabert, "Partial least squares identification of multi look-up table digital predistorters for concurrent dual-band envelope tracking power amplifiers," *IEEE Trans. Microw. Theory Techn.*, vol. 66, no. 12, pp. 5143–5150, Dec. 2018. doi: 10.1109/TMTT.2018.2857819.

[31] H. Cao, H. M. Nemati, A. Soltani Tehrani, T. Eriksson, and C. Fager, "Digital predistortion for high efficiency power amplifier architectures using a dual-input modeling approach," *IEEE Trans. Microw. Theory Techn.*, vol. 60, no. 2, pp. 361–369, Feb. 2012. doi: 10.1109/TMTT.2011.2176956.

[32] S. A. Bassam, M. Helaoui, and F. M. Ghannouchi, "Crossover digital predistorter for the compensation of crosstalk and nonlinearity in MIMO transmitters," *IEEE Trans. Microw. Theory Techn.*, vol. 57, no. 5, pp. 1119–1128, May 2009. doi: 10.1109/TMTT.2009.2017258.

[33] A. Abdelhafiz, L. Behjat, F. M. Ghannouchi, M. Helaoui, and O. Hammi, "A high-performance complexity reduced behavioral model and digital predistorter for MIMO systems with crosstalk," *IEEE Trans. Commun*, vol. 64, no. 5, pp. 1996–2004, May 2016. doi: 10.1109/TCOMM.2016.2545654.

[34] F. M. Barradas, P. M. Tomé, J. M. Gomes, T. R. Cunha, P. M. Cabral, and J. C. Pedro, "Power, linearity, and efficiency prediction for MIMO arrays with antenna coupling," *IEEE Trans. Microw. Theory Techn.*, vol. 65, no. 12, pp. 5284–5297, Dec. 2017. doi: 10.1109/TMTT.2017.2766067.

[35] Q. Luo, C. Yu, and X. W. Zhu, "Digital predistortion of phased array transmitters with multi-channel time delay," in *2018 IEEE Topical Conf. RF/Microwave Power Amplifiers for Radio and Wireless Applications (PAWR)*, Anaheim, CA, 2018, pp. 54–57.

[36] X. Liu et al. "Beam-oriented digital predistortion for 5G massive MIMO hybrid beamforming transmitters," *IEEE Trans. Microw. Theory Techn.*, vol. 66, no. 7, pp. 3419–3432, July 2018. doi: 10.1109/TMTT.2018.2830772.

[37] M. Abdelaziz, L. Anttila, A. Brihuega, F. Tufvesson, and M. Valkama, "Digital predistortion for hybrid MIMO transmitters," *IEEE J. Sel. Topics in Signal Process.*, vol. 12, no. 3, pp. 445–454, June 2018. doi: 10.1109/JSTSP.2018.2824981.

[38] M. N. Ruiz, A. L. Benito, J. R. Pérez-Cisneros, P. L. Gilabert, G. Montoro, and J. A. García, "Constant-gain envelope tracking in a UHF outphasing transmitter based on continuous-mode class-E GaN HEMT PAs," *2016 IEEE MTT-S Int. Microwave Symp. (IMS)*, San Francisco, CA, 2016, pp. 1–4.

[39] G. Wimpenny, "Envelope tracking PA characterisation," Open ET Alliance, Cambridge, U.K., White Paper, Nov. 2011.

[40] P. J. Brehm and T. W. Barton, "Modeling and analysis of the frequency dependence of class-E outphasing," in *Proc. 13th Int. Conf. Advanced Technologies, Systems and Services in Telecommunications (TELSIKS)*, 2017, pp. 170–173.

[41] H. Gheidi, P. Theilmann, J. J. Yan, T. Nakatani, and D. Kimball, "A broadband envelope-tracking push-pull GaN power amplifier using grounded-coplanar ring Marchand balun," in *Proc. 2018 IEEE 19th Wireless and Microwave Technology Conf. (WAMICON)*, Sand Key, FL, 2018, pp. 1–4.

[42] A. Cidronali, G. Manes, N. Giovannelli, T. Vlasits, and R. Hernaman, "Efficiency and linearity enhancements with envelope shaping control in dual-band envelope tracking GaAs PA," in *Proc. 6th European Microwave Integrated Circuit Conf.*, Manchester, U.K., 2011, pp. 308–311.

[43] J. Qureshi et al., "A 90-W peak power GaN outphasing amplifier with optimum input signal conditioning," *IEEE Trans. Microw. Theory Techn.*, vol. 57, no. 8, pp. 1925–1935, Aug. 2009. doi: 10.1109/TMTT.2009.2025430.

[44] P. L. Gilabert, D. López-Bueno, and G. Montoro, "Spectral weighting orthogonal matching pursuit algorithm for enhanced out-of-band digital predistortion linearization," *IEEE Trans. Circuits Syst. II, Express Briefs*, doi: 10.1109/TCSII.2018.2878581.

[45] D. López–Bueno, Q. A. Pham, G. Montoro, and P. L. Gilabert, "Independent digital predistortion parameters estimation using adaptive principal component analysis," *IEEE Trans. Microw. Theory Techn.*, vol. 66, no. 12, pp. 5771–5779, Dec. 2018. doi: 10.1109/TMTT.2018.2870420.

[46] M. N. Ruiz, R. Marante, L. Rizo, J. A. García, P. L. Gilabert, and G. Montoro, "A dual-band outphasing transmitter using broadband class E power amplifiers," in *Proc. 2014 Int. Workshop Integrated Nonlinear Microwave and Millimetre-Wave Circuits (INMMiC)*, Leuven, Belgium, 2014, pp. 1–3.

[47] P. H. Pednekar and T. W. Barton, "Dual-band Chireix combining network," in *Proc. 2016 Texas Symp. Wireless and Microwave Circuits and Systems (WMCS)*, Waco, TX, 2016, pp. 1–4.